Adhesion of membranes via switchable molecules

Bartosz Różycki,[1,2] Thomas R. Weikl,[1] and Reinhard Lipowsky[1]
[1]*Max Planck Institute of Colloids and Interfaces, Science Park Golm, 14424 Potsdam, Germany*
[2]*Institute of Theoretical Physics, Warsaw University, Hoża 69, 00 681 Warszawa, Poland*
(Received 17 March 2006; revised manuscript received 4 May 2006; published 16 June 2006)

Biomimetic membranes that adhere to a solid substrate or another interface via switchable crosslinker molecules are studied theoretically using analytical methods and Monte Carlo simulations. The flexible crosslinkers exhibit two conformations which have a different end-to-end distance and, thus, lead to different local separations of the membrane from the substrate surface. Transitions between the molecular conformations can be induced by light, electric potential, or changes in *p*H and lead to active shape fluctuations of the membrane and, thus, to an increased membrane roughness. The forward and backward transitions are characterized by two transition rates, ω_+ and ω_-, respectively, which define the average fraction $X=\omega_+/(\omega_++\omega_-)$ of + (or on) states and the mean switching rate $\omega=(\omega_++\omega_-)/2$. The membrane roughness is explicitly calculated as a function of X and ω. It is shown that the interplay of active and thermal fluctuations is subtle and that it is, in general, not possible to describe the active fluctuations in terms of an effective temperature.

DOI: 10.1103/PhysRevE.73.061908 PACS number(s): 87.16.Dg, 68.35.Np, 82.40.Np, 05.40.−a

I. INTRODUCTION

Biomimetic membranes such as lipid bilayers can be anchored to solid or fluid interfaces via a thin layer of polymers that act as flexible crosslinkers [1]. These polymers may form soft "cushions" of flexible tethers which are firmly attached both to the membrane and to the supporting interface [2,3]. In this paper, we theoretically consider such systems with the additional feature that the polymer layer contains switchable or stimulus-responsive molecular groups. These molecules exhibit several conformations and undergo transitions between these conformations which can be induced by light, electric potential, or changes in *p*H. Examples for such switchable molecules are provided by azobenzenes [4–6], pyrimidine-terminated molecules [7], (16-Mercapto) hexadecanoic acid [8], rotaxanes [9,10], and copolymers with polyethylene glycol side chains [11]. All of these molecules have been used to construct monolayers on solid substrates. In some cases, the changes in the hydrophobicity of the monolayers were studied by deposition of water droplets on top of these layers, in other cases, the monolayers were in contact with an aqueous solution; a recent review about these experiments is given in Ref. [12].

It is important to note that the induced transitions of a molecule between two possible conformations, say + and − or "on" and "off," represent a stochastic process. This process is governed by two transition rates, ω_+ and ω_-, for the forward and backward transition, respectively. In general, neighboring molecules will undergo these transitions in an asynchronous manner. Thus if we made several snapshots of the switchable surface, we would observe different patterns of "on" states. In a stationary state, these patterns evolve with time in such a way that the average fraction of "on" states remains constant and equal to $X\equiv\omega_+/(\omega_-+\omega_+)$.

Next, let us consider a biomimetic membrane that adheres to a solid substrate via a thin layer of polymers. We now imagine to integrate molecular switches into this layer and, in this way, obtain the ability to locally change the layer thickness. The "off" and "on" states now correspond to two different thicknesses, l_{off} and l_{on}, of the layer of crosslinkers, respectively. Thus if the crosslinker molecules undergo a transition from the "off" to the "on" state, the local membrane separation changes from l_{off} to l_{on} and back to l_{off} for the reverse transition. The membrane as a whole then undergoes active shape fluctuations that are induced by the conformational transitions of the flexible crosslinkers. In this paper, we address these active shape fluctuations and their interplay with thermally excited fluctuations from a theoretical point of view.

The flexible crosslinker molecules considered here differ from the relatively rigid stickers or adhesion molecules that we considered in a recent letter [13]. This latter study addressed the adhesion of membranes via stickers that are coupled to active processes such as ATP hydrolysis which switch the molecules between two conformational states. The sticker can bind the membrane only if it is in one of these conformational states. Therefore the effective membrane potential is switched locally between an attractive potential well and a repulsive potential. In the present case, the switching process leads to two different potential wells and, thus, to two different bound states depending on the extension of the crosslinkers. Switching between two bound membrane states is also relevant for biological membranes that are confined by external constraints such as the cytoskeleton and experience local time-dependent forces. One example is provided by the flickering of red blood cells [14,15]. In addition, the coupling of active processes to membranes has also been studied in the context of ion pumps, both theoretically [16–19] and experimentally [20], and for inclusions that act to change the local thickness [21] or curvature [22–24] of the membranes.

From the theoretical point of view, the systems studied here are interesting since they lead to a Langevin-type equation that involves *both* additive *and* multiplicative noise. The general distinction between these two types of noise is discussed in many textbooks of stochastic processes such as, e.g., [25–27]. For the systems considered here, the additive noise corresponds to the *thermal motion* of the membrane whereas the multiplicative noise describes the coupling of

the membrane to the *active switching process*. As we will show below, it is useful to distinguish two different cases: (i) The *symmetric* case for which the thermal roughness of the membrane has the same value for $X=0$, i.e., if all molecules are in the "off" state, and for $X=1$, i.e., if all molecules are in the "on" state; and (ii) the *asymmetric* case for which the membrane roughness differs in the two limiting cases $X=0$ and $X=1$. Case (ii) is certainly more realistic but case (i) is also useful since the corresponding theoretical model can be solved exactly.

In the symmetric case (i), the membrane roughness can be decomposed into a thermal and an active contribution. In the asymmetric case (ii), such a decomposition is no longer possible. We also show that the concept of an effective temperature is, in general, not applicable. For the membrane roughness, it only applies to the symmetric case. In addition, the probability distribution for the membrane separation has a single peak for high switching rates and two peaks for low switching rates. It thus exhibits a noise-induced transition [25] as a function of switching rate. Even in the symmetric case, such a transition cannot be understood in terms of the effective temperature for the membrane roughness.

Our paper is organized as follows. In Sec. II, we introduce our model for a fluctuating membrane that is crosslinked to a substrate surface covered by switchable molecules. The movement of such a membrane is described by a Langevin-type equation with both additive and multiplicative noise. In Sec. III, we discuss our Monte Carlo simulation method, which corresponds to the usual Metropolis algorithm, and provide an *explicit mapping* between the latter algorithm and the Langevin-type equation. In Sec. IV, we study the interplay between thermal motion and active switching between two molecular conformations. For the symmetric case, the Langevin-type equation is solved exactly. Using our explicit mapping, the exact solution provides a quantitative check on the accuracy of the computer simulations. For the asymmetric case, we describe a mean field approximation which reproduces the qualitative features of the simulation data.

II. MODEL

We consider a course-grained model that describes membranes as elastic sheets which form deformable but, on average, flat surfaces. The membrane shape is described by the local displacements from a planar reference state. Since we want, eventually, to study our model by computer simulations, the reference plane is divided into a square lattice with lattice constant a. Each lattice site is labeled by a pair of integer numbers $i=(x,y)$ with $1\leq x\leq N$, $1\leq y\leq N$ and periodic boundary conditions in both directions. The membrane displacement for lattice site i is denoted by l_i. The set $\{l\}$ of all N^2 local displacements thus specifies the membrane configuration. For any such configuration, the elastic energy of the membrane has the form [28,30]

$$\mathcal{H}_{\mathrm{el}}\{l\}=\sum_i \frac{\kappa}{2a^2}(\Delta_d l_i)^2, \tag{1}$$

where the parameter κ is the bending rigidity of the membrane, and the discretized Laplace operator $\Delta_d l_i$, which is defined via

$$\Delta_d l_{x,y}\equiv l_{x+1,y}+l_{x-1,y}+l_{x,y+1}+l_{x,y-1}-4l_{x,y}, \tag{2}$$

is equal to twice the local mean curvature of the membrane surface times a^2.

The membranes are taken to experience local and time-dependent forces which arise from active, i.e., energy-consuming processes in the environment of the membrane. In the systems considered here, the forces are generated by switchable molecules which bind the membrane to the planar substrate. In biological systems, such forces can be generated, for example, if the membrane interacts with cytoskeletal filaments or with adhesion molecules that undergo conformational changes [13].

These forces will be described by activity variables $s_i(t)$, which are defined locally at each lattice site i and change with time t. Therefore the potential energy of the membrane segment at site i, $V(l_i,s_i)$, depends both on the membrane displacement field l_i and on the local activity $s_i(t)$. It will also be useful to consider the potential energy per unit area, $V_{\mathrm{me}}(l_i,s_i)$, which is defined by

$$V(l_i,s_i)\equiv a^2 V_{\mathrm{me}}(l_i,s_i). \tag{3}$$

In the limit of small a, the potential energy density V_{me} stays finite whereas the potential energy V goes to zero.

If we combine the elastic energy of the membrane with its potential energy, we obtain the configuration energy (or effective Hamiltonian)

$$\mathcal{H}\{l,s\}=\mathcal{H}_{\mathrm{el}}\{l\}+\sum_i V(l_i,s_i)=\mathcal{H}_{\mathrm{el}}\{l\}+a^2\sum_i V_{\mathrm{me}}(l_i,s_i). \tag{4}$$

For a given activity pattern $\{s\}$, the statistical weight for membrane configuration $\{l\}$ at temperature T is then proportional to the Boltzmann factor $\exp[-\mathcal{H}\{l,s\}/k_BT]$.

A. Thermal motion

The membrane is embedded in an aqueous solution and is, thus, subject to thermal collisions with the water molecules. This leads to thermally excited deformations of the membrane shape [31–33]. In the framework of the geometric membrane models considered here, these deformations are described by changes in the membrane displacement field l. In general, there can be several mechanisms that contribute to the dissipation of the shape fluctuations of the membranes such as Stokes friction arising from the coupling to the surrounding liquid and interbilayer dissipation arising from the friction between the two adjacent monolayers [34]. We will consider the simplest type of dynamics which corresponds to the relaxation of the displacement variables along the gradients of the configuration energy $\mathcal{H}\{l\}$ of the membrane [28,30]. In the context of polymers and critical phenomena, this corresponds to Rouse dynamics [35] and to the so-called model A dynamics [36], respectively.

The corresponding Langevin equation is given by

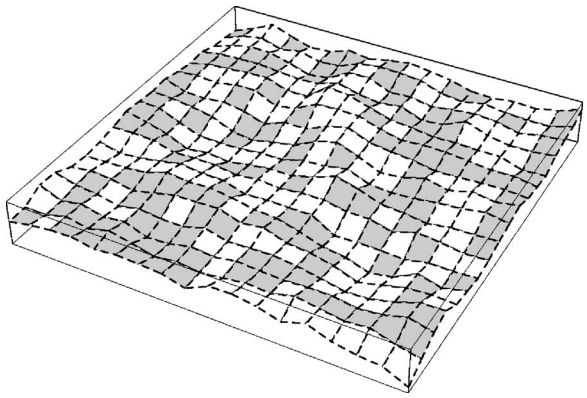

FIG. 1. Snapshot of a flexible membrane in a certain activity pattern $\{s\}$ which is defined, at each lattice site i, by a binary or Ising-like variable $s_i=\pm 1$. The white and gray membrane patches correspond to $s_i=-1$ and $s_i=+1$, respectively. The time evolution of the activity pattern is characterized by two transition rates as described in the text.

$$\phi\frac{\partial l_i}{\partial t}=-\frac{\partial \mathcal{H}}{\partial l_i}+\eta_i=-\frac{\kappa}{a^2}\Delta_d^2 l_i-\frac{\partial V(l_i,s_i)}{\partial l_i}+\eta_i, \tag{5}$$

which depends on the friction coefficient ϕ and describes the overdamped motion of the displacement variable l_i as a result of three types of forces: (i) the elastic restoring force $-\partial\mathcal{H}_{\rm el}/\partial l_i=-(\kappa/a^2)\Delta_d^2 l_i$ with

$$\Delta_d^2 l_i\equiv[(\partial^4/\partial x^4)_d+2(\partial^2/\partial x^2)(\partial^2/\partial y^2)_d+(\partial^4/\partial y^4)_d]l_{x,y}, \tag{6}$$

which couples l_i with the displacement variables at 12 neighboring lattice sites, (ii) the force $\partial V(l_i,s_i)/\partial l_i$ which arises from the potential V and depends on the value of the activity variable s_i, and (iii) the thermal white noise η_i. The average value of this latter noise vanishes at each lattice site, i.e.,

$$\langle\eta_i(t)\rangle=0, \tag{7}$$

and its correlation function is given by

$$\langle\eta_i(t)\,\eta_{i'}(t')\rangle=2\phi k_BT\delta(t-t')\,\delta_{i,i'} \tag{8}$$

as required by the fluctuation-dissipation theorem (or the principle of detailed balance).

B. Active processes

So far, we have not specified the activity variables s_i. A simple and natural choice is to take binary or Ising-like variables $s_i=\pm 1$ where $s_i=-1$ corresponds to the "off"-state and $s_i=+1$ corresponds to the "on"-state of the activity variable at lattice site i. A membrane segment with a certain activity pattern $\{s\}$ is shown in Fig. 1. This implies that the local force F_i experienced by the membrane segment at lattice site i is given by

$$F_i=-\partial V(l_i,-1)/\partial l_i \quad \text{for } s_i=-1 \text{ (inactive site)}$$
$$=-\partial V(l_i,+1)/\partial l_i \quad \text{for } s_i=+1 \text{ (active site)}.$$

In general, the activity patterns $\{s\}=\{s(t)\}$ could exhibit various spatial and temporal correlations. For simplicity, we will take the local activity fields $s_i(t)$ at different lattice sites to be statistically independent from each other and to have temporal correlations that decay with a single characteristic time scale. More precisely, we will consider, at each lattice site i, the so-called dichotomic process (or two-valued Markov process or random telegraph process) [27]. For this process, the probabilities $P_+(t)$ and $P_-(t)$ to find the activity variable $s_i(t)$ in the "on"- and "off"-state, respectively, satisfy the simple evolution equations

$$dP_+/dt=-P_+\omega_-+P_-\omega_+,$$

$$dP_-/dt=+P_+\omega_--P_-\omega_+,$$

which depends on the two transition rates ω_+ and ω_-. The transition rate ω_+ represents the probability per unit time to go from the "off"-state $s_i=-1$ to the "on"-state $s_i=+1$. Likewise, the transition rate ω_- represents the probability per unit time for the reverse process from the "on"-state $s_i=+1$ to the "off"-state $s_i=-1$. These transition rates are taken to be the same for all lattice sites i and for all values of the membrane displacement field l_i.

In order to discuss the statistical properties of this active process, it will be convenient to use the variable

$$X\equiv\frac{\omega_+}{\omega_++\omega_-}, \tag{9}$$

which describes the average fraction of "on" sites, and the mean switching rate

$$\omega\equiv\frac{\omega_++\omega_-}{2} \tag{10}$$

instead of the two transition rates ω_+ and ω_-. Here and below, X and ω will be considered as the basic *switching parameters*. In terms of X and ω, the stationary probability distribution $P^{(\rm st)}(s_i)$ for each of the statistically independent activity fields s_i is given by

$$P^{(\rm st)}(s)=X\delta_{s,1}+(1-X)\,\delta_{s,-1}. \tag{11}$$

Furthermore, the variables $s_i(t)$ have the average value

$$\langle s_i(t)\rangle=2X-1 \tag{12}$$

and the two-point correlation function

$$\langle s_i(t)s_{i'}(t')\rangle-\langle s_i(t)\rangle\langle s_{i'}(t')\rangle=4X(1-X)e^{-2\omega|t-t'|}\delta_{i,i'}. \tag{13}$$

The angular brackets in Eqs. (12) and (13) represent averages with respect to the stationary distribution as given by Eq. (11). Note that the correlation function (13) of the activity variables decays exponentially with the decay time $1/2\omega$.

C. Thermal versus active fluctuations

If $\omega_+=0$, all activity fields are switched off and $X=0$; if $\omega_-=0$, all activity fields are switched on and $X=1$. In these two special cases, the correlation function (13) is identically zero, and the Langevin dynamics as given by Eq. (5) describes the relaxation of the membrane displacements in the

laterally uniform potentials $V(l,1)$ and $V(l,-1)$, respectively. The membrane will then attain a certain equilibrium state and relax to the deepest potential well after a sufficiently long time. In such an equilibrium state, the displacement variables l_i will undergo thermal fluctuations which are governed by the thermal energy k_BT.

In general, we will consider active processes which are characterized by an "on" fraction X with $0<X<1$ and a mean switching rate ω with $0<\omega<\infty$. These processes induce additional membrane fluctuations which are *not* governed by the thermal energy k_BT but by the switching parameters X and ω. In general, the overall membrane fluctuations may be dominated by thermal fluctuations or by active fluctuations or both contributions may be comparable. In the case of actively switched harmonic potentials as studied in Sec. IV below, the membrane roughness can be explicitly decomposed into a thermal and into an active part. One can then determine the range of X and ω values for which the active fluctuations dominate.

A rather intuitive concept for the coupling to active processes is the idea that these processes can be described in terms of an effective temperature (see, e.g., [37]). Thus, in the present context, one might be tempted to think that the additional membrane fluctuations, which are induced by the active switching of the membrane potential, correspond to fluctuations at a higher, effective temperature. However, this effective temperature concept is only applicable (i) for certain observables and (ii) for a limited range of model parameters as we will show explicitly for the case of actively switched harmonic potentials.

III. SIMULATION METHODS

The statistical properties of the membrane models introduced in the previous section can be studied by Monte Carlo simulations [38]. It is then useful to introduce the length scale

$$l_{\mathrm{sc}} \equiv a\sqrt{k_BT/\kappa} \tag{14}$$

and to define the dimensionless displacement variable [28]

$$z_i \equiv l_i/l_{\mathrm{sc}} = (l_i/a)\sqrt{\kappa/k_BT} \tag{15}$$

at lattice site i. It is instructive to estimate the length scale l_{sc} for phospholipid bilayers. In this case, the bending rigidity is of the order of $20k_BT$ and the lattice parameter a is of the order of 6 nm [29]. This implies that $l_{\mathrm{sc}} \simeq 1.3$ nm.

The membrane shape is now specified by the set $\{z\}$ and the configuration energy (4) is rewritten in terms of these variables. As before, we consider a discrete lattice of $N\times N$ sites. Each lattice site is labeled by a pair of integer numbers $i=(x,y)$ with $1\le x\le N$, $1\le y\le N$ and periodic boundary conditions in both the x and the y directions. The Monte Carlo (MC) simulations described here have been performed with up to 10^8 MC steps, i.e., MC moves per lattice site.

Each MC move consists of two submoves: (i) First, a lattice site, i, is randomly chosen, and the membrane position at this site, z_i, is shifted to the value $z_i+\zeta$, where ζ is a random number with the probability distribution $p(\zeta)=1/(2\delta z)$ for $-\delta z<\zeta<\delta z$, and δz is the step size for the displacement variable. This submove is accepted according to the standard Metropolis algorithm with probability

$$w\{z\to z'\} = \min(1, e^{-[\mathcal{H}\{z',s\}-\mathcal{H}\{z,s\}]/k_BT}) \tag{16}$$

where the new, primed displacement fields are defined by $z_j' \equiv z_j + \delta_{i,j}\zeta$; and (ii) the second submove consists of the random choice of another lattice site j for which the value of the activity variable s_j is switched from $s_j=1$ to $s_j=-1$ with probability Ω_- and vice versa with probability Ω_+.

It has been previously argued that the Metropolis algorithm has the same scaling properties as the Langevin dynamics [28] since both describe the relaxational dynamics along the gradients of the configuration energy. However, we will now show that it is even possible to derive a *quantitative* mapping between the Metropolis algorithm just described and the Langevin dynamics as given by Eq. (5). This mapping is obtained in the limit of small δz, i.e., of small step size for the displacement variables z_i, and leads to explicit relations between the simulation parameters $\delta z, \Omega_+, \Omega_-$ and the parameters ϕ, ω_+, ω_-, which appear in the continuous time model.

In order to derive this mapping, let us consider the probability distribution $P\{z,s,t\}$ for the membrane configuration $\{z\}$ and the activity pattern $\{s\}$ at time t. The probability current density $I_i\{z,s,t\}$, which is induced by the first submove (i) as described above with $z\equiv z_i$, satisfies the master equation

$$I_i\{z,s,t\}\delta t = \frac{1}{2\delta z}\int_{-\delta z}^{\delta z} d\zeta [P\{z',s,t\}w\{z'\to z\} - P\{z,s,t\}w\{z\to z'\}] \tag{17}$$

with the time step δt corresponding to one submove and the transition probabilities $w\{z'\to z\}$ as in Eq. (16). The first and second terms in the square bracket describe the gain and loss of the probability density, respectively. In order to make a connection with the continuous time model corresponding to the Langevin dynamics (5), we will now consider the limit of small time step δt and small step size δz for the displacement variables.

We thus expand the probability distribution P and the transition probabilities w, which are present on the right-hand side of Eq. (17), in powers of the dimensionless variable ζ which is then integrated between $-\delta z$ and $+\delta z$. In order to perform this expansion in a systematic way, one has to take into account that the transition probabilities as given by Eq. (16) are not differentiable at $\zeta=0$ and, thus, lead to two different expressions for $\zeta<0$ and $\zeta>0$. The most transparent way to keep track of the different terms is to distinguish several cases depending on the sign of $\partial\mathcal{H}/\partial z_i$. Expansion of the integrand up to second order in ζ and subsequent integration over ζ leads to the truncated master equation

$$I_i\{z,s,t\}\delta t = \frac{(\delta z)^2}{6}\frac{\partial}{\partial z_i}\left(\frac{1}{k_BT}\frac{\partial \mathcal{H}}{\partial z_i}+\frac{\partial}{\partial z_i}\right)P\{z,s,t\}+O[(\delta z)^3]. \tag{18}$$

On the other hand, the probability current density which corresponds to the Langevin dynamics for the membrane separation field l_i as given by Eq. (5) has the Smoluchowski or Fokker-Planck form

$$I_i\{l,s,t\} = \frac{1}{\phi}\frac{\partial}{\partial l_i}\left(\frac{\partial \mathcal{H}}{\partial l_i}+k_BT\frac{\partial}{\partial l_i}\right)P\{l,s,t\}. \tag{19}$$

Comparing the two expressions in Eqs. (18) and (19) and using the relation $z=(l/a)(\kappa/k_BT)^{1/2}$ as in Eq. (15), we obtain the parameter relation

$$\delta t = \frac{(\delta z)^2}{6}\frac{\phi a^2}{\kappa}. \tag{20}$$

If this relation is fulfilled, the Langevin dynamics as given by Eq. (5) and the Metropolis dynamics as in Eq. (16) are equivalent in the limit of small step size $\delta z \sim (\delta t)^{1/2}$.

Since we alternate between submove (i) and submove (ii), the same time step δt is used for both submoves. This implies that the switching probabilities $\Omega_\pm$ and the transition rates $\omega_\pm$ are related via

$$\Omega_\pm = \delta t\,\omega_\pm = \frac{(\delta z)^2}{6}\frac{\phi a^2}{\kappa}\omega_\pm. \tag{21}$$

In the next section, we will apply this simulation method to the active switching between two bound states. We will distinguish two cases which we call the symmetric and the asymmetric case. For the symmetric case, both bound states lead to the same thermally excited roughness of the membrane. In contrast, the asymmetric case is characterized by two bound states that differ in their thermal roughness.

In both cases, the system attains a steady state which is characterized by certain time-independent quantities such as the average membrane separation $\langle z_i\rangle$ and the two-point correlation function $\langle z_i z_{i'}\rangle - \langle z_i\rangle\langle z_{i'}\rangle$. A useful test for our simulation code is provided by the symmetric case since we can obtain an explicit analytical solution for this case. The corresponding analytical expressions are compared with the simulation results in Figs. 3–5. Inspection of these figures shows that, for sufficiently small simulation step sizes δz, the statistical properties of the membrane model are determined by our simulations with rather high accuracy.

For all Monte Carlo simulations reported below, the step size δz was chosen to be $\delta z=0.025$. In addition, we used the system sizes $N=40$ or $N=60$ and checked that these sizes are sufficiently large so that our data are not affected by finite size effects.

IV. ACTIVE SWITCHING BETWEEN TWO BOUND STATES

A. Crosslinkers with two molecular conformations

Let us now consider a membrane which is immobilized on a planar substrate surface. The connection between the membrane and the substrate is provided by anchored polymers which act as flexible crosslinkers [2,3]. The end-to-end distance of the polymers is equal to the local separation of the membrane from the substrate. Now, let us imagine to integrate switchable or stimulus-responsive molecular groups into these crosslinkers. For simplicity, we will assume that each crosslinker can attain only two different conformations, which we call "on" and "off" (or "up" and "down") and which differ in their end-to-end distance $l_{\rm on}$ and $l_{\rm off}$. Thus, depending on the molecular conformation, the local separation of the membrane from the substrate is $l_{\rm off}$ or $l_{\rm on}$. In addition, we assume that we can switch the molecular conformation by an external signal such as light, electric potential, or pH.

For such a system, the "off" conformation leads to an effective membrane potential $V(l_i,-1)$ with a local minimum at $l_i=l_{\rm off}$ whereas the "on" conformation implies another membrane potential $V(l_i,+1)$ with a local minimum at $l_i=l_{\rm on}$. The "off-on" transition, which occurs with transition rate ω_+ is induced by the external signal whereas the "on-off" transition can occur spontaneously with transition rate ω_-. In the following, we will use the convention that $l_{\rm on}>l_{\rm off}$; the opposite case with $l_{\rm on}<l_{\rm off}$ can be easily obtained by permuting the two indices.

In order to obtain a tractable model, we now expand the effective potentials $V(l_i,-1)$ and $V(l_i,+1)$ around their minima up to second order in the displacement variables which leads to

$$V(l_i,s_i=-1) \approx V_{\rm off}+\frac{1}{2}v_-(l_i-l_{\rm off})^2 \tag{22}$$

and

$$V(l_i,s_i=+1) \approx V_{\rm on}+\frac{1}{2}v_+(l_i-l_{\rm on})^2 \tag{23}$$

with $V_{\rm off}\equiv V(l_{\rm off},-1)$ and $V_{\rm on}\equiv V(l_{\rm on},+1)$. It is then convenient to transform the displacement variables l_i according to $l_i\to l_i'\equiv l_i+l_{\rm off}v_-/(v_-+v_+)+l_{\rm on}v_+/(v_-+v_+)$. If we denote the shifted variables l_i' again by l_i, we obtain

$$V(l_i,s_i=-1) = V_{\rm off}+\frac{1}{2}v_-(l_i+l_-)^2$$

$$\text{with } l_- \equiv (l_{\rm on}-l_{\rm off})\frac{v_+}{v_-+v_+} \tag{24}$$

and

$$V(l_i,s_i=+1) = V_{\rm on}+\frac{1}{2}v_+(l_i-l_+)^2$$

$$\text{with } l_+ \equiv (l_{\rm on}-l_{\rm off})\frac{v_-}{v_-+v_+}. \tag{25}$$

The shift of the displacement variables l_i was done in such a way that the two parameters l_- and l_+ satisfy the simple relation

$$v_-l_- = v_+l_+. \tag{26}$$

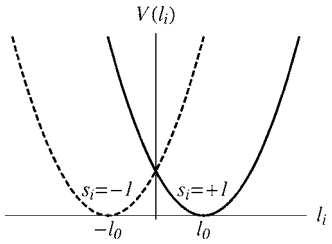

FIG. 2. Symmetric switching: Two harmonic potentials V as a function of the displacement variable l_i at lattice site i. If the activity variable $s_i=-1$, the harmonic potential is located at $l=-l_0$; if the activity variable $s_i=+1$, the potential is located at $l=+l_0$.

The two harmonic potentials as given by Eqs. (24) and (25) imply the local force

$$F_i = -v_-(l_i + l_-)\tfrac{1}{2}(1 - s_i) - v_+(l_i - l_+)\tfrac{1}{2}(1 + s_i) = -\tfrac{1}{2}(v_- + v_+)l_i + \tfrac{1}{2}(v_- - v_+)s_i l_i + v_+ l_+ s_i$$

acting on the membrane segment at lattice site i where relation (26) has been used in the second line. If this local force is inserted into the general Langevin equation as given by Eq. (5), we obtain the stochastic equation of motion

$$\phi\frac{\partial l_i}{\partial t} + \frac{\kappa}{a^2}\Delta_d^2 l_i + \frac{v_- + v_+}{2}l_i - \frac{v_- - v_+}{2}s_i l_i = v_+ l_+ s_i + \eta_i \tag{27}$$

for the displacement variable l_i at lattice site i. As before, the time evolution of l_i depends (i) on the thermal force η_i, (ii) on the activity variable s_i, and (iii) on the neighboring displacement variables which are coupled to l_i via the curvature term proportional to κ. Note that the absolute values V_{off} and V_{on} of the membrane potentials at l_{off} and l_{on} do not enter the local forces and, thus, do not enter the Langevin equation.

The two terms on the right-hand side of Eq. (27) represent *additive* noise terms whereas the last term on the left-hand side is proportional to the product $s_i l_i$ and, thus, corresponds to a *multiplicative* noise term. For the special case of *symmetric switching* with $v_+=v_-$, the multiplicative noise term vanishes which leads to the explicit solution described in the next section.

B. Symmetric case

Let us now focus on the symmetric case for which the two harmonic potentials $V(l_i,-1)$ and $V(l_i,+1)$ in Eqs. (24) and (25) have the same "spring constants" given by

$$v_+ = v_- \equiv v \tag{28}$$

which also implies

$$l_+ = l_- \equiv l_0 \tag{29}$$

via relation (26). The two harmonic potentials are shown in Fig. 2 where we have set $V_{\text{off}}=0$ and $V_{\text{on}}=0$ since these parameters do not enter the Langevin equation. The effective membrane potential now has the particularly simple form

$$V(l_i,s_i) = \tfrac{1}{2}v(l_i - s_i l_0)^2 \tag{30}$$

and the Langevin equation (27) reduces to

$$\phi\frac{\partial l_i}{\partial t} + \frac{\kappa}{a^2}\Delta_d^2 l_i + v l_i = v l_0 s_i + \eta_i \tag{31}$$

with two additive noise terms on the right-hand side but no multiplicative noise term.

The local energy input provided by the activity variables s_i onto the membrane segment at site i can be estimated as follows. In the off state with $s_i=-1$, the membrane segment will try to attain the local displacement $l_i=-l_0$ corresponding to the minimum of the effective membrane potential $V(l_i,-1)$. If the activity variable is now switched to $s_i=+1$, this membrane segment attains the potential energy $V(-l_0,+1)=2vl_0^2$. The latter energy has to be provided by the activity variable which represents an external force field. For all parameter values discussed in the following, the local energy input $2vl_0^2$ is smaller or comparable to 10 k_BT.

1. Fourier decomposition

In order to handle the coupling between neighboring displacement variables, which arises from the curvature term, we now decompose the displacement variables $l_i=l_{x,y}$ with $1\le x\le N$ and $1\le y\le N$ into their Fourier components. This is possible since the sites (x,y) form an $N\times N$ lattice with periodic boundary conditions. The Fourier components or displacement modes are defined by

$$\tilde{l}_{m,n}(t) \equiv \frac{1}{N}\sum_{x=1}^{N}\sum_{y=1}^{N} e^{-2\pi i(xm+yn)/N} l_{x,y}(t), \tag{32}$$

where the two indices m and n satisfy $1\le m\le N$ and $1\le n\le N$. The Fourier decomposition is then given by

$$l_{x,y}(t) = \frac{1}{N}\sum_{m=1}^{N}\sum_{n=1}^{N} e^{2\pi i(xm+yn)/N}\tilde{l}_{m,n}(t). \tag{33}$$

Note that, in the exponents, the symbol $i\equiv\sqrt{-1}$ denotes the imaginary unit which should not be confused with the lattice site i. Likewise, we decompose the activity variables $s_{x,y}(t)$ and the thermal force $\eta_{x,y}(t)$ into their Fourier components, $\tilde{s}_{m,n}(t)$ and $\tilde{\eta}_{m,n}(t)$. When these Fourier series are inserted into the Langevin equation (31), we obtain the decoupled equations

$$\phi\left(\frac{\partial}{\partial t} + R_{m,n}\right)\tilde{l}_{m,n}(t) = \tilde{s}_{m,n}(t)vl_0 + \tilde{\eta}_{m,n}(t), \tag{34}$$

with the inverse relaxation time

$$R_{m,n} \equiv \frac{v}{\phi} + \frac{\kappa}{a^2\phi}Q_{m,n}^4 \tag{35}$$

for mode (m,n), and the dimensionless wave numbers

$$Q_{m,n} \equiv \left[4 - 2\cos\left(\frac{2\pi n}{N}\right) - 2\cos\left(\frac{2\pi m}{N}\right) \right]^{1/2}. \quad (36)$$

The linear equation of motion as given by Eq. (34), which describes the time evolution of the displacement modes $\tilde{l}_{m,n}$, has the general solution

$$\tilde{l}_{m,n}(t) = e^{-tR_{m,n}} \left[\tilde{l}_{m,n}(0) + \frac{1}{\phi} \int_0^t dt' e^{t'R_{m,n}} [\tilde{s}_{m,n}(t') v l_0 + \tilde{\eta}_{m,n}(t')] \right]. \quad (37)$$

Since the wave numbers $Q_{m,n}$ have the symmetry property $Q_{-m,-n}=Q_{m,n}$, one has

$$R_{-m,-n} = R_{m,n} \quad (38)$$

for the inverse relaxation times $R_{m,n}$. Furthermore, because of $0 \le Q_{m,n} \le 2\sqrt{2}$, the relaxation times $1/R_{m,n}$ satisfy the inequalities

$$\frac{\phi}{v} \frac{1}{1 + 64\kappa/a^2 v} \le \frac{1}{R_{m,n}} \le \frac{\phi}{v}. \quad (39)$$

2. Average membrane position

The average membrane position can be determined as follows. First, we take the average of both sides of Eq. (37). The average value $\langle \tilde{\eta}_{m,n}(t) \rangle = 0$ since the thermal white noise has been defined with $\langle \eta_{x,y} \rangle = 0$, see Eq. (7). For the two-valued Markov process, we have $\langle \tilde{s}_{m,n}(t) \rangle = (2X-1) N \delta_{m,N} \delta_{n,N}$ as follows from Eq. (12). Using these relations and performing the t' integration in Eq. (37), we get an explicit expression for $\langle \tilde{l}_{m,n}(t) \rangle$. In the long time limit, the system relaxes into its stationary state, and the average displacement variables attain the asymptotic values

$$\langle \tilde{l}_{m,n} \rangle \approx (2X-1) \frac{v l_0 N}{\phi R_{m,n}} \delta_{m,N} \delta_{n,N}. \quad (40)$$

Applying the discrete Fourier transform (33) to this equation, we find that, in the steady state, the average membrane position is given by

$$\langle l_i \rangle = \langle l_{x,y} \rangle \approx (2X-1) l_0, \quad (41)$$

which is independent of the mean switching rate ω but increases linearly with X as shown in Fig. 3. This behavior can also be obtained from the following simple argument. For the symmetric case, the membrane potential as given by Eq. (30) has two minima at $l_i = s_i l_0$ with $s_i = \pm 1$. Taking the average of both sides of this latter equation leads to $\langle l_i \rangle = (2X-1) l_0$, since $\langle s_i \rangle = 2X-1$. However, this simple relation is no longer valid for the asymmetric case which will be considered further below.

3. Average membrane roughness

The average membrane roughness $\xi_\perp$ can be obtained from the cumulant

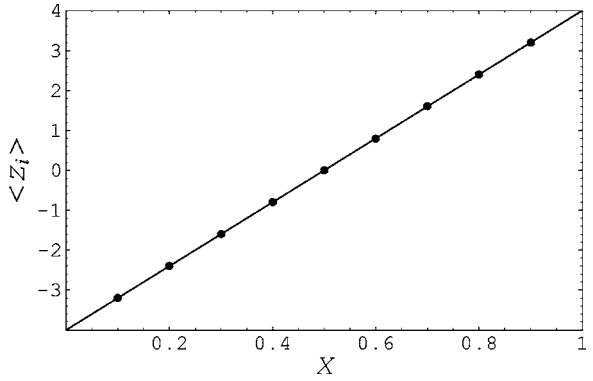

FIG. 3. The average membrane position $\langle z_i \rangle$, given in dimensionless units, for the steady state as a function of the average fraction X of the active crosslinker molecules with $s_i = 1$. The points represent data from Monte Carlo simulations while the solid line is obtained from Eq. (41). The mean switching rate ω is constant and given by $\omega \phi a^2/\kappa = 1$ with friction coefficient ϕ, molecular size a, and bending rigidity κ. The dimensionless distance between the two potential minima is $z_0 = 4$ and the rescaled spring constant $v a^2/\kappa = 1/5$.

$$\langle l_{x,y}(t)^2 \rangle_c \equiv \langle l_{x,y}(t)^2 \rangle - \langle l_{x,y}(t) \rangle^2 \quad (42)$$

which behaves as

$$\langle l_{x,y}(t)^2 \rangle_c \approx \xi_\perp^2 \quad \text{for large } t. \quad (43)$$

It is again convenient to use the Fourier transformed displacement variables $\tilde{l}_{m,n}$ which lead to

$$\langle l_{x,y}(t)^2 \rangle_c = \frac{1}{N^2} \sum_m \sum_n e^{-2\pi i (mx+ny)/N} \times \sum_{m'} \sum_{n'} e^{-2\pi i (m'x+n'y)/N} \langle \tilde{l}_{m,n}(t) \tilde{l}_{m',n'}(t) \rangle_c. \quad (44)$$

Using the general solution (37) for the displacement variables $\tilde{l}_{m,n}$, we can now express these variables in terms of $\tilde{s}_{m,n}(t')$, which describes the two-valued Markov process, and $\tilde{\eta}_{m,n}(t')$, which represents the thermal white noise. The latter variables have the correlation functions

$$\langle \tilde{\eta}_{m,n}(t) \tilde{\eta}_{m',n'}(t') \rangle = 2\phi k_B T \delta(t-t') \delta_{m,-m'} \delta_{n,-n'} \quad (45)$$

and

$$\langle \tilde{s}_{m,n}(t) \tilde{s}_{m',n'}(t') \rangle - \langle \tilde{s}_{m,n}(t) \rangle \langle \tilde{s}_{m',n'}(t') \rangle = 4X(1-X) e^{-2\omega|t-t'|} \delta_{m,-m'} \delta_{n,-n'} \quad (46)$$

as follows from Eqs. (8) and (13), respectively. In this way, we obtain an explicit expression for the cumulant $\langle l_{x,y}(t)^2 \rangle_c$ as given by Eq. (44). In the limit of large t, this expression leads to the average membrane roughness

$$\xi_\perp^2 = \frac{1}{N^2}\sum_{m=1}^{N}\sum_{n=1}^{N}\frac{1}{v+\frac{\kappa}{a^2}Q_{m,n}^4}\left(k_BT + \frac{4X(1-X)v^2l_0^2}{2\phi\omega + v + \frac{\kappa}{a^2}Q_{m,n}^4}\right). \tag{47}$$

Note that the first term on the right-hand side is proportional to the thermal energy k_BT whereas the second term depends on the switching parameters, X and ω, and is invariant under the transformation $X \to 1-X$ which arises from the symmetry of the underlying membrane potential as given by Eq. (30).

For $X=0$ or $X=1$, all molecules are in the off and on state, respectively, and the membrane stays in the corresponding minimum of the effective potential (30). In this case, the second term in Eq. (47) vanishes and the membrane roughness reduces to the thermal roughness $\xi_\perp = \xi_{\perp,\mathrm{th}}$ with

$$\xi_{\perp,\mathrm{th}}^2 \equiv \frac{1}{N^2}\sum_{m=1}^{N}\sum_{n=1}^{N}\frac{k_BT}{v+\frac{\kappa}{a^2}Q_{m,n}^4}. \tag{48}$$

For $0<X<1$, the molecules are actively switched and the membrane is locally displaced by these molecules. This leads to the additional, active roughness $\xi_{\perp,\mathrm{ac}}$ as given by

$$\xi_{\perp,\mathrm{ac}}^2 \equiv \frac{1}{N^2}\sum_{m=1}^{N}\sum_{n=1}^{N}\frac{4X(1-X)v^2l_0^2}{\left(v+\frac{\kappa}{a^2}Q_{m,n}^4\right)\left(2\phi\omega + v + \frac{\kappa}{a^2}Q_{m,n}^4\right)} \tag{49}$$

corresponding to the second term in Eq. (47). Note that the active roughness $\xi_{\perp,\mathrm{ac}}$ does not depend on temperature T. Thus, for the symmetric membrane potential considered here, the roughness can be decomposed into two contributions, a thermal and an active one, according to

$$\xi_\perp^2 = \xi_{\perp,\mathrm{th}}^2 + \xi_{\perp,\mathrm{ac}}^2. \tag{50}$$

The analytical result (47) for the membrane roughness is compared with Monte Carlo simulations in Figs. 4 and 5. In Fig. 4, the roughness is shown as a function of the average fraction X whereas Fig. 5 shows the ω dependence of this quantity.

The membrane roughness $\xi_\perp$ is a decreasing function of the mean switching rate ω, as shown in Fig. 5. This follows directly from Eq. (47) and can be intuitively understood as follows. The random force $F_{0,i}(t) \equiv v l_0 s_i(t)$, which appears on the right-hand side of Eq. (31), has a constant magnitude and acts in a given direction, on average, over the time period $1/\omega$. This time scale should be compared with the relaxation times $1/R_{m,n}$ for the displacement modes $\tilde{l}_{m,n}$. These relaxation times satisfy the inequalities as given by Eq. (39). If $1/\omega$ is shorter than the smallest membrane relaxation time, the random force $F_0 \equiv \{F_{0,i}\}$ cannot displace the membrane much from its average position and, thus, $\xi_\perp \approx \xi_{\perp,\mathrm{th}}$. In fact, in the limit of large switching rates, the actively induced roughness $\xi_{\perp,\mathrm{ac}}$ vanishes, and the membrane roughness as given by Eq. (47) becomes equal to the thermal roughness, $\xi_\perp = \xi_{\perp,\mathrm{th}}$. On the other hand, if $1/\omega$ is larger than the relaxation time for short-wavelength membrane deformations, the random forces F_0 act to increase the membrane roughness. The force centers in the state $s_i=-1$ keep pushing the membrane towards the potential minimum which is located at $l_i=-l_0$ while the force centers in the state $s_i=+1$ act to localize the membrane in the other potential minimum, at $l_i=l_0$. The membrane is then pulled between the two competitive minima of the external potential and its roughness is larger than in thermal equilibrium. The two regimes—of fast and slow switching—are separated by the longest membrane relaxation time which, according to relations (39), is equal to ϕ/v. This crossover is visible in Fig. 5 which shows the functional dependence of the membrane roughness on the switching rate; the midpoint between maximal and minimal roughness is located at switching rate $\omega = v/\phi$. Note that the

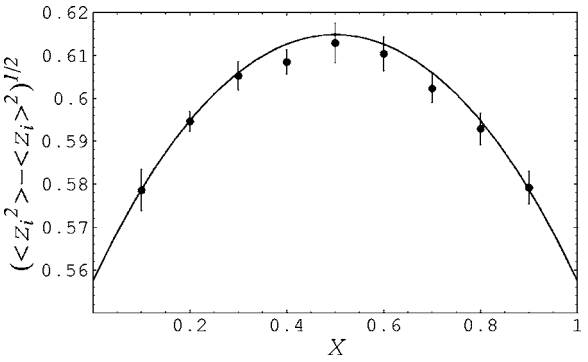

FIG. 4. The dimensionless membrane roughness $(\langle z_i^2\rangle - \langle z_i\rangle^2)^{1/2}$ in the steady state as a function of the average fraction X of crosslinker molecules that are in their active states with $s_i=1$. The points are obtained from simulations while the solid line shows relation (47). The model parameters are the same as in Fig. 3. The relative simulation error, in comparison to the exact result, is smaller than 1%. Note that the roughness is symmetric with respect to $X=1/2$.

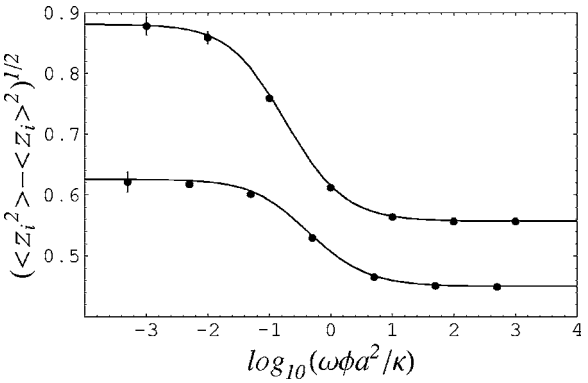

FIG. 5. The dimensionless membrane roughness $(\langle z_i^2\rangle - \langle z_i\rangle^2)^{1/2}$ in the steady state as a function of the average switching rate ω which is rescaled with the friction coefficient ϕ, the molecular size a, and the bending rigidity κ (semilogarithmic plot). The points represent Monte Carlo data and the solid lines are obtained from Eq. (47). For the upper curve, the dimensionless distance between the two harmonic potentials is $z_0=4$, and the rescaled spring constant $va^2/\kappa=1/5$. For the bottom curve, one has $z_0=2$ and $va^2/\kappa=1/2$. In both cases, the average fraction of the crosslinker molecules in their "on" state is $X=0.5$.

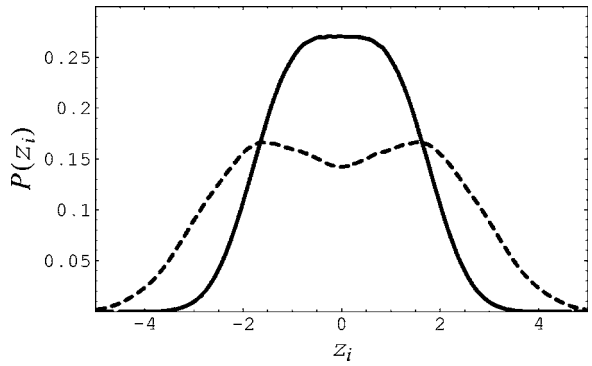

FIG. 6. The stationary probability distribution $P(z_i)$ for finding a membrane patch at position z_i. The two diagrams show results of our Monte Carlo simulations: the solid and dashed line corresponds to the switching rate $\omega=1.67v/\phi$ and $\omega=0.17v/\phi$, respectively, where v denotes the spring constant and ϕ is the friction coefficient. At frequency $\omega=v/\phi$ the probability distribution $P(z_i)$ exhibits a noise-induced transition from a distribution with a single maximum to a bimodal distribution with two maxima, which cannot be understood in terms of the active temperature $T_{\rm ac}$ as given by Eq. (65). Here, the average fraction of crosslinker molecules in their "on" state is $X=0.5$, the dimensionless distance between the two potential minima is $z_0=5$, and the spring constant v is given by $va^2/\kappa=6$ with the lattice constant a and the bending rigidity κ.

plot in Fig. 5 is semilogarithmic: a linear plot would lead to a functional dependence that is convex upwards for all values of the switching rate.

The above considerations indicate that the probability distribution $P(l_i)$ for finding a membrane patch in the steady state at position l_i should exhibit a noise-induced transition from a distribution with a single-peak to a bimodal distribution. At high switching rates the distribution $P(l_i)$ has a single maximum at $l_i=\langle l_i\rangle$ while at low switching frequencies it could have two maxima, one shifted towards $l_i=l_0$ and another one shifted towards $l_i=-l_0$. The transition should occur at $\omega=v/\phi$. These expectations are confirmed by our simulations, see Fig. 6.

4. Thermally versus actively induced roughness

In order to compare the relative size of the thermally and the actively induced roughness of the membrane, it is convenient to rewrite the corresponding expressions (48) and (49) for $\xi_{\perp,\rm th}$ and $\xi_{\perp,\rm ac}$ as follows. First, the thermal contribution $\xi^2_{\perp,\rm th}$ as given by Eq. (48) can be rewritten as

$$\xi^2_{\perp,\rm th}=a^2\frac{k_BT}{\kappa}f_1\left(\frac{va^2}{\kappa}\right), \tag{51}$$

where the function f_1 is defined by

$$f_1(\beta)\equiv\frac{1}{N^2}\sum_{m=1}^{N}\sum_{n=1}^{N}\frac{1}{\beta+Q^4_{m,n}}. \tag{52}$$

The actively induced roughness $\xi_{\perp,\rm ac}$ as given by Eq. (49) can also be expressed in terms of the function f_1 which leads to

$$\xi^2_{\perp,\rm ac}=a^2 4X(1-X)\frac{l_0^2v^2}{2\omega\phi\kappa}\left[f_1\left(\frac{va^2}{\kappa}\right)-f_1\left(\frac{2\omega\phi a^2}{\kappa}+\frac{va^2}{\kappa}\right)\right]. \tag{53}$$

The function f_1 as defined by Eq. (52) becomes particularly transparent if we consider the continuum limit of small lattice constant a and large system size Na. In the latter limit, the dimensionless wave numbers $Q_{m,n}$ as in Eq. (36) behave as

$$Q^2_{m,n}\approx a^2q^2 \tag{54}$$

with the two-dimensional momenta

$$\mathbf{q}\equiv(q_x,q_y)\equiv\left(\frac{2\pi m}{Na},\frac{2\pi n}{Na}\right). \tag{55}$$

Note that $Q^2_{m,n}\approx a^2q^2$ as in Eq. (54) ensures that the discrete elastic energy of the membrane as given by Eq. (1) has the correct continuum limit

$$\mathcal{H}_{\rm el}\{l\}=\int dxdy\tfrac{1}{2}\kappa(\nabla^2 l)^2. \tag{56}$$

Higher order terms arising from the expansion of the cosine terms in Eq. (36) reflect the discretization via a square lattice and have no significance for fluid membranes.

Inserting the asymptotic equality $Q_{m,n}\approx a^2q^2$ into Eq. (52) and replacing the sum by an integral, we obtain

$$f_1(\beta)\approx\frac{1}{a^2}\int\frac{d^2q}{(2\pi)^2}\frac{1}{(\beta/a^4)+q^4}\approx\frac{1}{8\sqrt{\beta}} \tag{57}$$

since the large momentum cutoff $\simeq\pi/a$ becomes infinite for small a.

If the asymptotic form (57) for the function f_1 is inserted in the expression (51), the thermal roughness becomes

$$\xi^2_{\perp,\rm th}\approx a\frac{k_BT}{\kappa}\frac{1}{8}\left(\frac{\kappa}{v}\right)^{1/2} \tag{58}$$

in the limit of small a and large N. If we considered the potential energy density $V_{\rm me}(l_i,s_i)=V(l_i,s_i)/a^2$ as introduced in Eq. (3), the harmonic potential (30) would have the form

$$V_{\rm me}(l,s)=\tfrac{1}{2}v_2(l-sl_0)^2\quad\text{with } v_2\equiv v/a^2. \tag{59}$$

In terms of $v=v_2a^2$, the thermal roughness becomes

$$\xi^2_{\perp,\rm th}\approx\frac{k_BT}{\kappa}\frac{1}{8}\left(\frac{\kappa}{v_2}\right)^{1/2} \tag{60}$$

which is independent of a.

For the actively induced roughness as given by Eq. (53), the continuum limit leads to

$$\xi^2_{\perp,\rm ac}\approx aX(1-X)\frac{l_0^2}{2}\left(\frac{v}{\kappa}\right)^{1/2}\left[f_2\left(\frac{2\omega\phi}{v}\right)\right]^{-1} \tag{61}$$

with the function

$$f_2(\gamma)\equiv 1+\gamma+\sqrt{1+\gamma}. \tag{62}$$

If we again replaced the potential parameter v by $v_2=v/a^2$, we would find that $\xi_{\perp,\rm ac}\sim a^2$. Thus, in contrast to the thermal

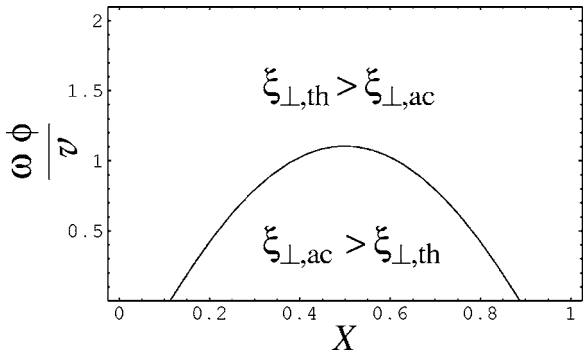

FIG. 7. Rescaled crossover rate $\omega=\omega_*$ as a function of the fraction X of the crosslinker molecules in their "on" states where ϕ and υ are the friction coefficient and the spring constant, respectively. The example shown here follows from the implicit equation (63) for local energy input $2l_0^2\upsilon=10k_BT$. For switching rates $\omega>\omega_*(X)$ and $\omega<\omega_*(X)$, the membrane roughness is dominated by thermal motion and active switching, respectively.

roughness, the actively induced roughness goes to zero in the limit of small a and fixed υ_2 which reflects the molecular nature of the switchable crosslinkers.

We now define the crossover rate ω_* by the requirement that the thermal and the actively induced roughness are equal, i.e., $\xi_{\perp,\mathrm{th}}^2=\xi_{\perp,\mathrm{ac}}^2$, for this crossover rate. Using the expressions (58) and (61), which are valid for large N, we obtain the implicit equation

$$f_2\left(\frac{2\omega_*\phi}{\upsilon}\right)=4X(1-X)\frac{l_0^2\upsilon}{k_BT} \tag{63}$$

for the crossover rate ω_*. Note that this equation depends only on three dimensionless parameters: the rescaled switching rate $2\omega_*\phi/\upsilon$, the average fraction X of on states, and the rescaled local energy input $2l_0^2\upsilon/k_BT$. If we keep the latter parameter fixed, the solution of Eq. (63) leads to a functional dependence of the crossover rate ω_* on X as schematically shown in Fig. 7. For switching rates $\omega>\omega_*(X)$ and $\omega<\omega_*(X)$, the membrane roughness is dominated by thermal motion and active switching, respectively.

5. Active switching and effective temperature

It is instructive to see to what extent the active switching of the crosslinker molecules can be described by an effective temperature. Comparison of the two expressions (58) and (61) for the thermally and actively induced membrane roughness shows that

$$\xi_{\perp,\mathrm{ac}}^2=\xi_{\perp,\mathrm{th}}^2(T=T_{\mathrm{ac}}) \tag{64}$$

if one considers the thermal roughness $\xi_{\perp,\mathrm{th}}$ as a function of temperature T and defines the active temperature $T_{\mathrm{ac}}=T_{\mathrm{ac}}(X,\omega)$ via

$$k_BT_{\mathrm{ac}}\equiv 4X(1-X)l_0^2\upsilon\left[f_2\left(\frac{2\omega\phi}{\upsilon}\right)\right]^{-1}, \tag{65}$$

which depends both on the switching parameters, X and ω, and on the potential parameters, υ and l_0. The total membrane roughness can then be written as

$$\begin{aligned}\xi_\perp^2&=\xi_{\perp,\mathrm{th}}^2(T)+\xi_{\perp,\mathrm{ac}}^2=\xi_{\perp,\mathrm{th}}^2(T)+\xi_{\perp,\mathrm{th}}^2(T_{\mathrm{ac}})\\&=\xi_{\perp,\mathrm{th}}^2(T_{\mathrm{eff}}\equiv T+T_{\mathrm{ac}}).\end{aligned} \tag{66}$$

It is important to note, however, that the effective temperature $T_{\mathrm{eff}}=T+T_{\mathrm{ac}}$ does not apply to other quantities such as the probability distribution for the displacement field l that undergoes a transition from a single peak distribution to a bimodal distribution with two peaks.

C. Asymmetric case

Let us now return to the stochastic equation of motion (27) and consider the asymmetric case of two harmonic potentials with two different spring constants $\upsilon_+\neq\upsilon_-$. Because of the multiplicative noise term, s_il_i, we are no longer able to solve Eq. (27) analytically. In order to get some insight into the more general case $\upsilon_+\neq\upsilon_-$, we now perform a mean-field-type approximation and replace the term s_il_i in Eq. (27) by $(2X-1)l_i$, i.e., we replace the stochastic variable s_i by its average value $2X-1$. By doing this, we reduce the stochastic equation (27), containing both additive and multiplicative noise terms, to Eq. (31) with additive noise only, provided we identify

$$\upsilon\equiv X\upsilon_+ + (1-X)\upsilon_- \tag{67}$$

and

$$l_0\equiv\frac{l_+\upsilon_+}{X\upsilon_+ + (1-X)\upsilon_-}. \tag{68}$$

In the symmetric case with $\upsilon_+=\upsilon_-$, the above relations are equivalent with the previous definitions (28) and (29).

Within the framework of the mean-field approximation (MFA), that we have introduced above, the average membrane position and roughness are determined by Eqs. (41) and (47), respectively, with υ and l_0 as given by relations (67) and (68). Note that for $X=1$, Eqs. (67) and (68) reduce to $\upsilon=\upsilon_+$ and $l_0=l_+$, while for $X=0$, we get $\upsilon=\upsilon_-$ together with $l_0=l_-$, since $\upsilon_+l_+=\upsilon_-l_-$. These limiting cases are understandable. For $X=1$ all lattice sites remain in the on state with harmonic potential (25), while for $X=0$ all sites are in the off state and potential (24). Thus, in these two cases, we expect the MFA to be exact. In particular, in these two cases we get the correct thermal roughness for membranes within the corresponding harmonic potential.

To verify the accuracy of the MFA, we compare its predictions with simulation results. Examples are shown in Figs. 8–10. Our simulation data indicate that the MFA gives the correct formula for the average membrane position

$$\langle l_i\rangle=\frac{(2X-1)l_+\upsilon_+}{X\upsilon_+ + (1-X)\upsilon_-}, \tag{69}$$

see also Fig. 8. For $X=0$ and $X=1$ the above equation reduces to exact values $\langle l_i\rangle=l_-$ and $\langle l_i\rangle=l_+$, respectively. Moreover, $\langle l_i\rangle$ is an increasing function of X, which is rather plausible: the more lattice sites are in the on state, the stronger is the membrane pulled towards the potential minimum located at $l_i=l_+$. Note also that for the symmetric case with $\upsilon_+=\upsilon_-$, Eq. (69) reduces to the linear X dependence (41).

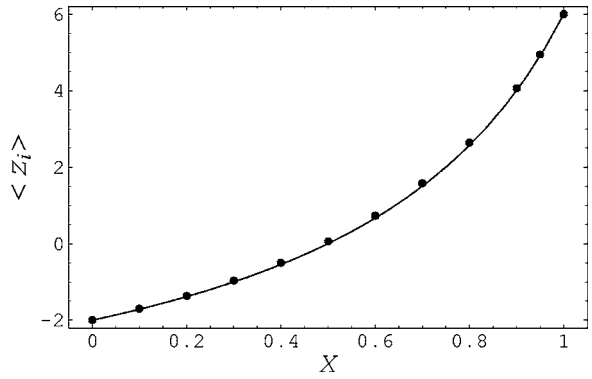

FIG. 8. The average membrane position $\langle z_i \rangle$, given in dimensionless units, as a function of the average fraction X of crosslinker molecules in the "on" state. The points represent Monte Carlo data and the solid line shows relation (69) which is determined from the MFA. The mean switching rate ω is constant and, as in Fig. 3, given by $\omega\phi a^2/\kappa=1$ with friction coefficient ϕ, lattice constant a, and bending rigidity κ. The minima of potentials (24) and (25) are located at $z_+=6$ and $z_-=2$, whereas the spring constants v_+ and v_- are given by $v_+a^2/\kappa=0.2$ and $v_-a^2/\kappa=0.6$, so that the parameter relation (26) is fulfilled.

The effective parameters v and l_0, as given by Eqs. (67) and (68), do not depend on ω but only on X. Thus, if one now considers the membrane roughness $\xi_\perp$, the ω dependence remains the same as in the symmetric case (i.e., $\xi_\perp$ is a decreasing function of the switching rate) whereas one has a more complex X dependence. One consequence of this is that, when plotted as a function of X, the roughness is no longer symmetric with respect to $X=1/2$, see Fig. 9.

In the mean-field approximation used here, the membrane roughness $\xi_\perp$ is given by

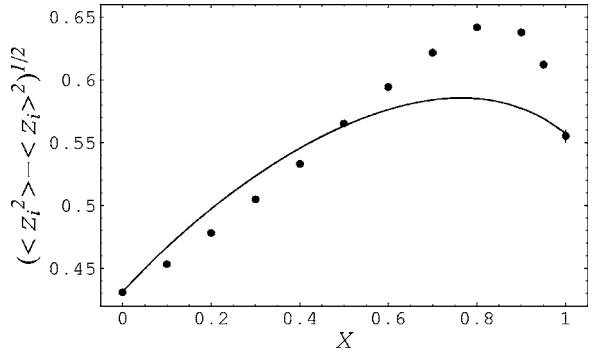

FIG. 9. The dimensionless roughness $(\langle z_i^2\rangle-\langle z_i\rangle^2)^{1/2}$ of the membrane in the steady state is shown as a function of the average fraction X of the "on" crosslinker molecules. The points are obtained from MC simulations and the solid line shows relation (70) which is determined from the MFA. The MFA is exact for $X=0$, $X=1$, and $X=1/2$. The model parameters are the same as in Fig. 8. Note also that the membrane roughness is no longer symmetric with respect to $X=1/2$.

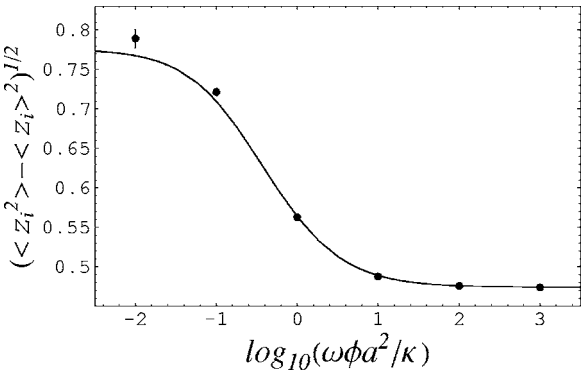

FIG. 10. The membrane roughness $(\langle z_i^2\rangle-\langle z_i\rangle^2)^{1/2}$, given in dimensionless units, as a function of the mean switching rate ω which is rescaled with the friction coefficient ϕ, the lattice constant a, and the bending rigidity κ (semilogarithmic plot). In this example, the average fraction of crosslinker molecules in their "on" state is $X=1/2$. Other model parameters are the same as in Figs. 8 and 9. The points represent data from our MC simulations and the solid line is obtained from Eq. (70). The MFA is correct over a wide range of switching rates ω.

$$\xi_\perp^2 = a^2\frac{k_BT}{\kappa}f_1\left(\frac{va^2}{\kappa}\right) + a^2 4X(1-X)\frac{l_0^2v^2}{2\omega\phi\kappa}\left[f_1\left(\frac{va^2}{\kappa}\right) - f_1\left(\frac{va^2}{\kappa}+\frac{2\omega\phi a^2}{\kappa}\right)\right], \tag{70}$$

with v and l_0 as in Eqs. (67) and (68). This expression for $\xi_\perp^2$ increases with temperature T and decreases with the mean switching rate ω, as in the symmetric case. However, it can no longer be decomposed into thermally and actively induced contributions, since even the first term in Eq. (70) which is proportional to k_BT now depends on the switching parameter X, see Eq. (67). It is therefore impossible to extend the definition (64) of the active temperature T_{ac} to the asymmetric case.

In Figs. 9 and 10, we show the average membrane roughness $\xi_\perp$ as a function of the switching parameters X and ω, respectively, and compare results obtained from the MFA and simulations. Our simulation data show that the MFA leads to the roughness $\xi_\perp$ that is exact for $X=0$ and $X=1$, and presumably for $X=1/2$ as well (see Fig. 10). This result is clear since for $X=0$ and $X=1$ Eq. (70) gives the correct thermal roughness $\xi_{\perp,\mathrm{th}}$ for membranes in the harmonic potentials (24) and (25), respectively. For other X values, the MFA remains only in qualitative agreement with the simulation results. If the stiffer harmonic potential dominates, the MF roughness is too small compared to the simulation data. If the softer harmonic potential dominates, then the MF roughness is too large compared to the simulation results.

In Fig. 11 we show the stationary probability distribution $P(l_i)$ for finding a membrane patch at distance l_i from the substrate. The two sets of data were obtained from Monte Carlo simulations: the gray and black points correspond to the switching rate $\omega<v/\phi$ and $\omega>v/\phi$, respectively, where the potential parameter v is given by Eq. (67), and ϕ denotes the friction coefficient. At $\omega=v/\phi$ the probability distribu-

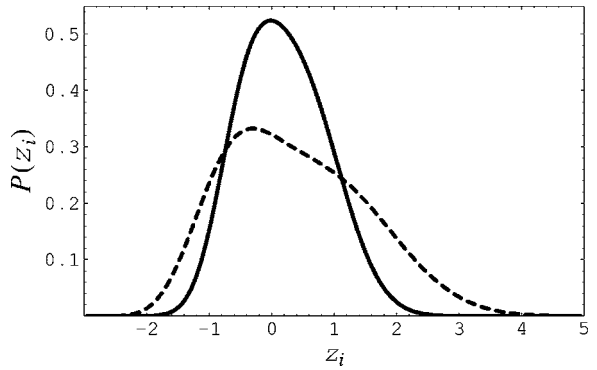

FIG. 11. The stationary probability distribution $P(z_i)$ for finding a membrane patch at position z_i. The two sets of data show results of our MC simulations: the dashed and solid line corresponds to the switching rate $\omega=0.25v/\phi$ and $\omega=2v/\phi$, respectively, where v is the effective parameter given by Eq. (67) and ϕ denotes the friction coefficient. At $\omega=v/\phi$ the probability distribution $P(z_i)$ exhibits a noise-induced transition from a distribution with a single peak to a bimodal distribution. Here, the average fraction of crosslinker molecules in their "on" state is $X=0.5$. The minima of potentials (24) and (25) are located at $z_+=6$ and $z_-=2$ whereas the spring constants v_+ and v_- are given by $v_+a^2/\kappa=2$ and $v_-a^2/\kappa=6$, so that the parameter relation (26) is fulfilled.

tion $P(l_i)$ exhibits a noise-induced transition from an almost symmetric to a highly asymmetric function.

V. SUMMARY AND OUTLOOK

We have presented a simple theoretical model for biomimetic membranes that are bound to a planar substrate by anchored polymers which act as flexible crosslinkers. These crosslinkers can attain two different conformations that differ in their end-to-end distance. In addition, the crosslinker molecules are switchable, and one can induce transitions between their two conformations by an external signal such as light, electric potential, or changes in pH. The membrane then exhibits active shape fluctuations which lead to an increase of the membrane roughness.

The conformational transitions of the crosslinker molecules as well as the thermal motion of the membrane in an aqueous solution represent stochastic processes. Therefore the model dynamics is stochastic and given by the Langevin-type equation (5) that describes the overdamped motion of the membrane displacement field, and the two-valued Markov process that describes random transitions between the two possible conformational states, denoted by "on" and "off," of the crosslinker molecules.

The two-valued Markov process is characterized by two switching rates, ω_+ and ω_-, for the forward and backward transitions, respectively. These transition rates define the mean switching rate $\omega=(\omega_++\omega_-)/2$ and the average fraction $X=\omega_+/(\omega_++\omega_-)$ of "on" molecules in a steady state. Using both analytical methods and Monte Carlo simulations, we have determined the average membrane position and membrane roughness as a function of the switching parameters, X and ω, and temperature T. These calculations were done for two different types of effective membrane potentials: (i) Symmetric ones for which the two potential wells acting on the membrane have the same shape and (ii) asymmetric ones for which these two potential wells differed in their shape. In case (i), the Langevin-type equation contains only an additive noise term, in case (ii) this equation involves both additive and multiplicative noise.

In the symmetric case (i) we have solved the Langevin-type equation analytically in Fourier space and found exact expressions for the average membrane position and for the membrane roughness, see Figs. 3–5. These exact results provide a useful test for our simulation methods. In this case, we could decompose the membrane roughness into a thermal and an active contribution as given by Eqs. (58) and (61), respectively. This allows us to determine the range of X and ω values for which the active fluctuations dominate over the thermal ones and, additionally, to introduce a natural definition of an effective temperature T_{eff}. Using Monte Carlo simulations we have also determined the stationary probability distribution for finding a membrane patch at a given distance from the substrate surface as shown in Fig. 6. This distribution has a single maximum if the switching process is sufficiently fast, while for low switching rates ω it has two separated maxima. It thus exhibits a noise-induced transition which, however, cannot be understood in terms of the effective temperature T_{eff}.

In the asymmetric case (ii) we are not able to solve the Langevin-type equation analytically. To find an approximate solution of this equation we have applied a mean-field theory that leads to an expression for the average membrane position which seems to be exact as confirmed by Monte Carlo simulations, see Fig. 8. The mean-field expression for the roughness, on the other hand, is only qualitatively correct, see Fig. 9. Furthermore, it is no longer possible to decompose the membrane roughness into a thermally and actively induced contribution.

It is straightforward to generalize our results to tense membranes and interfaces. For an effective membrane tension σ, we obtain the modified relaxation rate

$$R_{m,n}=\frac{v}{\phi}+\frac{\sigma}{\phi}Q_{m,n}^2+\frac{\kappa}{a^2\phi}Q_{m,n}^4 \tag{71}$$

which generalizes the expression (35) used above. One then has to distinguish a rigidity-dominated regime with tension $\sigma<\sigma_*\equiv\sqrt{4\kappa v/a^2}$ from a tension-dominated regime with tension $\sigma>\sigma_*$ [39]. In the rigidity-dominated regime, the tension is irrelevant and one recovers the system behavior as obtained in the present paper; in the tension-dominated regime, on the other hand, the bending rigidity is irrelevant and the system behavior will be different. In fact, in the tension-dominated regime, thermally excited membrane fluctuations are strongly suppressed which implies an enlarged parameter region, for which active switching dominates the membrane roughness, compare Fig. 7. This latter modification also applies to the shape fluctuations of interfaces governed by interfacial tension.

Finally, let us come back to the experimental systems mentioned in the Introduction. Several types of polymers

have been used as crosslinkers between membranes and substrate surfaces [2,3], and it seems feasible to integrate switchable molecular groups into these polymers. One example for such a group is provided by azobenzene chromophores that can be switched between a low energy *trans* and a high energy *cis* configuration. The spatial displacement associated with such a conformational transition is relatively small and of the order of 2 Å. Thus, in order to have an appreciable effect onto the end-to-end distance of the crosslinkers, one would have to incorporate several such groups into each crosslinker.

Larger changes in the end-to-end distance can be achieved by other molecular architectures such as, e.g., copolymers consisting of polymethacrylic acid (PMAA) and polyethylene glycol (PEG). These copolymers undergo a conformational transition from a relatively compact structure at low *p*H to a relatively open or swollen structure at high *p*H. Layers of such copolymers in aqueous solution have been recently studied by atomic force microscopy [11]. The thickness of these layers could be changed between 2 and 14 nm by changing the *p*H of the solution between *p*H 4 and *p*H 9. Furthermore, fast and reversible changes of the *p*H can be achieved by photolysis of phenolic compounds [40].

In our study, the change in polymer layer thickness or membrane/substrate separation is equal to $2l_0=2z_0l_{sc}\simeq 2.6z_0$ nm where the latter estimate corresponds to phospholipid bilayers, compare Eq. (14). In the simulations, we have chosen a relatively large value for z_0 in order to suppress statistical errors. The value $z_0=2$, for example, corresponds to a change of 5.2 nm in the polymer layer thickness. However, the general relations (69) and (70) for the average membrane separation and the membrane roughness apply for any value of z_0. As far as the roughness is concerned, inspection of Eq. (70) shows that this quantity depends only on the combination $2vl_0^2$ which represents the local energy input provided by the active switching process.

In the numerical example shown in Fig. 7, the local energy input was chosen to be $10k_BT$. This represents the energy which is needed in order to stretch or compress the flexible parts of the crosslinker. This energy input is typically smaller than the energy needed in order to switch the conformation of the molecular group. The energy barrier for the *trans/cis* transition of one azobenzene chromophore, e.g., is of the order of 20 k_BT [41]. For a light-induced process, both the elastic deformation of the crosslinkers and the switching of the molecular groups will be provided by the absorbed photons. This is quite feasible since, for visible light, a single photon provides an energy input between 60 and 100 k_BT.

ACKNOWLEDGMENT

B.R. would like to thank Marek Napiórkowski for stimulating and useful discussions.

[1] E. Sackmann, Science **271**, 43 (1996).
[2] M. L. Wagner and L. K. Tamm, Biophys. J. **79**, 1400 (2000).
[3] C. A. Naumann *et al.*, Biomacromolecules **3**, 27 (2002).
[4] M. S. Ferritto and D. A. Tirrell, Macromolecules **21**, 3117 (1988).
[5] G. Möller, M. Harke, and H. Motschmann, Langmuir **14**, 4955 (1998).
[6] K. Ichimura, S.-K. Oh, and M. Nakagawa, Science **288**, 1624 (2000).
[7] S. Abbott, J. Ralston, G. Reynolds, and R. Hayes, Langmuir **15**, 8923 (1999).
[8] H. Lahann *et al.*, Science **299**, 371 (2003).
[9] R. A. Bissell, E. Córdova, A. E. Kaifer, and J. F. Stoddart, Nature (London) **369**, 133 (1994).
[10] J. Berna *et al.*, Nat. Mater. **4**, 704 (2005).
[11] M. Ye, D. Zhang, L. Han, J. Tejada, and C. Ortiz, Soft Mater. **2**, 243 (2006).
[12] Y. Liu, L. Mu, B. Liu, and J. Kong, Chem.-Eur. J. **11**, 2622 (2005).
[13] B. Różycki, R. Lipowsky, and T. R. Weikl, Phys. Rev. Lett. **96**, 048101 (2006).
[14] S. Tuvia, S. Levin, A. Bitler, and R. Korenstein, J. Cell Biol. **141**, 1551 (1998).
[15] N. S. Gov and S. A. Safran, Biophys. J. **88**, 1859 (2005).
[16] J. Prost and R. Bruinsma, Europhys. Lett. **33**, 321 (1996).
[17] R. Granek and S. Pierrat, Phys. Rev. Lett. **83**, 872 (1999).
[18] D. Lacoste and A. W. C. Lau, Europhys. Lett. **70**, 418 (2005).
[19] L. C.-L. Lin, N. Gov, and F. L. H. Brown, J. Chem. Phys. **124**, 074903 (2006).
[20] J.-B. Manneville, P. Bassereau, D. Levy, and J. Prost, Phys. Rev. Lett. **82**, 4356 (1999).
[21] M. C. Sabra and O. G. Mouritsen, Biophys. J. **74**, 745 (1998).
[22] S. Ramaswamy, J. Toner, and J. Prost, Phys. Rev. Lett. **84**, 3494 (2000).
[23] H.-Y. Chen, Phys. Rev. Lett. **92**, 168101 (2004).
[24] R. Reigada, J. Buceta, and K. Lindenberg, Phys. Rev. E **71**, 051906 (2005).
[25] W. Horsthemke and R. Lefever, *Noise–Induced Transitions*, 1st ed. (Springer-Verlag, Berlin, 1984).
[26] H. Risken, *The Fokker-Planck Equation: Methods of Solution and Applications* (Springer-Verlag, Berlin, 1989).
[27] N. van Kampen, *Stochastic Processes in Physics and Chemistry* (Elsevier, Amsterdam, 1992).
[28] R. Lipowsky and B. Zielinska, Phys. Rev. Lett. **62**, 1572 (1989).
[29] R. Goetz, G. Gompper, and R. Lipowsky, Phys. Rev. Lett. **82**, 221 (1999).
[30] T. R. Weikl and R. Lipowsky, Phys. Rev. E **64**, 011903 (2001).
[31] J. O. Rädler, T. J. Feder, H. H. Strey, and E. Sackmann, Phys. Rev. E **51**, 4526 (1995).
[32] B. Pozo-Navas, V. A. Raghunathan, J. Katsaras, M. Rappolt, K. Lohner, and G. Pabst, Phys. Rev. Lett. **91**, 028101 (2003).
[33] H-G. Döbereiner, G. Gompper, C. K. Haluska, D. M. Kroll, P. G. Petrov, and K. A. Riske, Phys. Rev. Lett. **91**, 048301 (2003).
[34] U. Seifert and S. A. Langer, Europhys. Lett. **23**, 71 (1993);

Biophys. Chem. **49**, 13 (1994).
[35] M. Doi and S. F. Edwards, *The Theory of Polymer Dynamics* (Clarendon Press, Oxford, 1986).
[36] P. C. Hohenberg and B. I. Halperin, Rev. Mod. Phys. **49**, 435 (1977).
[37] R. D. Vale and F. Oosawa, Adv. Biophys. **26**, 97 (1990).
[38] K. Binder and D. W. Heermann, *Monte Carlo Simulation in Statistical Physics* (Springer-Verlag, Berlin, 1992).
[39] R. Lipowsky, in *Structure and Dynamics of Membranes*, edited by R. Lipowsky and E. Sackmann (Elsevier, Amsterdam, 1995), p. 521.
[40] M. Gutman, D. Huppert, and E. Pines, J. Am. Chem. Soc. **103**, 3709 (1981).
[41] A. R. Dias *et al.*, J. Chem. Thermodyn. **24**, 439 (1992).